frontiers | Frontiers in Detector Science and Technology

TYPE Original Research
PUBLISHED 22 December 2023
DOI 10.3389/fdest.2023.1282854

OPEN ACCESS

EDITED BY
Gabriele Croci,
University of Milano-Bicocca, Italy

REVIEWED BY
Carlo Cazzaniga,
United Kingdom Research and Innovation, United Kingdom
Ettore Segreto,
State University of Campinas, Brazil

*CORRESPONDENCE
P. Amedo,
pablo.amedo@gmail.com

RECEIVED 24 August 2023
ACCEPTED 08 December 2023
PUBLISHED 22 December 2023

CITATION
Amedo P, González-Díaz D, Brunbauer FM, Fernández-Posada DJ, Oliveri E and Ropelewski L (2023), Observation of strong wavelength-shifting in the argon-tetrafluoromethane system. *Front. Detect. Sci. Technol* 1:1282854. doi: 10.3389/fdest.2023.1282854

Observation of strong wavelength-shifting in the argon-tetrafluoromethane system

P. Amedo[1]*, D. González-Díaz[1], F. M. Brunbauer[2], D. J. Fernández-Posada[1], E. Oliveri[2] and L. Ropelewski[2]

[1]Galician Institute of High Energy Physics (IGFAE), Universidade de Santiago de Compostela, Santiago de Compostela, Spain, [2]European Council for Nuclear Research (CERN), Geneva, Switzerland

We report the scintillation spectra of Ar/CF_4 mixtures in the range 210–800 nm, obtained under X-ray irradiation for various pressures (1–5 bar) and concentrations (0%–100%). Special care was taken to eliminate effects related to space charge and charge recombination, so that results can be extrapolated following conventional wisdom to those expected for minimum ionizing particles under the typical electric fields employed in gaseous instrumentation. Our study sheds light into the microscopic pathways leading to scintillation in this family of mixtures and reinvigorates the prospects of use in next-generation scintillation-based chambers.

KEYWORDS

gaseous detectors, time projection chambers, scintillators, scintillation and light emission processes (solid, gas and liquid scintillators), CF_4, argon, noble gas mixtures, gas scintillation

1 Introduction

Since their introduction in 1974 (Nygren, 2023), time projection chambers (TPCs) have proved to be one of the most effective ways of detecting particles and reconstructing their trajectories. The versatility of these devices, being compatible with *B*-fields, allowing readout flexibility and a wide range of density media (from some 10's of mbar up to 10's of bar, liquid or even solid phase), makes them the perfect tool to study many different phenomena in particle physics (González-Díaz et al., 2018).

Gas-based TPCs commonly operate with admixtures of noble gases with some molecular species, chiefly CH_4, i-C_4H_{10}, CF_4 or CO_2. TPCs make use of these additives to reduce the spatial spread and collection time of the primary ionization, minimize photon and ion feedback and, in general, to attain a greater stability. Among them, CF_4 exhibits some particularly interesting properties such as intense and broadband scintillation in the range 150–750 nm under primary (Pansky et al., 1995; Morozov et al., 2010; Morozov et al., 2011) and secondary (field-assisted) (Fraga et al., 2003; Morozov et al., 2012; González-Díaz, 2016) particle excitation, and very low electron diffusion (Christophorou and Olthoff, 2004). The VUV-visible scintillation yields induced by α particles in pure CF_4 are found in the range 1,000–3,000 ph/MeV (Pansky et al., 1995; Azmoun et al., 2010; Morozov et al., 2010; Lehaut et al., 2015), optical gains well above 10^4 have been reported in CF_4-based mixtures in González-Díaz (2016), while diffusion coefficients have been shown to remain at the thermal limit up to pressure-reduced drift fields as high as 1 kV/cm/bar (Christophorou and Olthoff, 2004).

Based on the aforementioned observations, CF_4 by itself makes an interesting TPC gas [and has been used to that aim before, e.g., (Takahashi et al., 2011; Battat et al.,

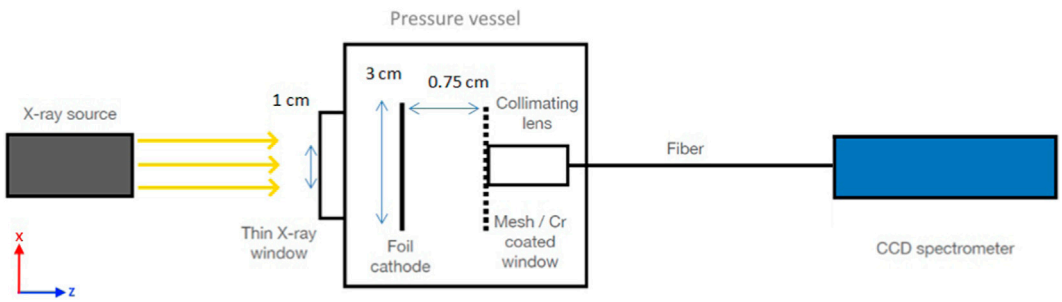

FIGURE 1
Schematic drawing of the experimental setup used to conduct the measurements. The x-ray tube is shown to the left, the high-pressure vessel housing the electrifiable scintillating cylinder is shown at the middle. The spectrophotometer is shown to the right.

2014)]. In fact, CF_4 either pure or admixed with other elements is of great contemporary interest to the optical imaging of rare processes in low-pressure gases (Baracchini et al., 2020; Araújo et al., 2023). Ar/CF_4 admixtures, in particular, have been pioneered by the Fraga and Fraga group at Coimbra already in the 00's for optical imaging (Fraga et al., 2001; Fraga et al., 2002), and revived recently in an optical-TPC demonstrator equipped with a triple-stack of gas electron multipliers (GEMs), (González-Díaz, 2016; Brunbauer et al., 2018). These works consistently showed a higher optical gain compared to pure CF_4, with indirect evidence for wavelength-shifting reactions between Ar states and the CF_4 scintillation precursors. Besides the enhanced performance of Ar/CF_4 mixtures for GEM operation, argon is considerably more cost-effective and environment-friendly than CF_4. Compared to a traditional wavelength-shifter like N_2, main advantages of CF_4 are its strong scintillation in the visible range together with a much lower electron diffusion, potentially allowing sharper and brighter tracks from CMOS and CCD cameras, e.g., when instrumenting optical TPCs in the field of nuclear physics (Pomorski et al., 2014; Zimmerman, 2023).

Argon has another characteristic relevant to modern instrumentation: it is the element of choice of the DUNE experiment, where it acts simultaneously as target and detection medium both at its far and near detector complexes (Abi et al., 2020). Specifically, an argon-rich high pressure TPC capable of reconstructing low-energy hadrons (down to 10's of MeV, at least) has been proposed by the collaboration (Abed Abud, 2023). It is called to be the first detector to ever record neutrino interactions in a sparse medium, with 4π coverage and broad particle identification (PID) capabilities. In this context, enabling time-tagging through the primary scintillation produced in neutrino interactions, while preserving the argon medium as pure as possible (to avoid parasitic neutrino interactions), is the subject of ongoing investigations (Amedo, 2021; Saá-Hernández, 2023). Time tagging is an essential asset in the study of neutrino oscillations with TPCs as it is used for spill-assignment, absolute estimate of the drift distance and time-of-flight determination of the emerging particles (Manly et al., 2021).

With this in mind, we performed a systematic study of the primary scintillation in the Ar/CF_4 system down to trace-amounts of the molecular additive, in order to better understand its wavelength-shifting capabilities. For that, a spectroscopic analysis was carried out under X-ray irradiation at varying pressures and CF_4 concentrations, at electric fields and ionization densities for which space charge and charge/light recombination effects are negligible. Following conventional wisdom (e.g. Menzel, 2014; Azevedo et al., 2018), measurements in these conditions should represent a good approximation to the scintillation by minimum ionizing particles, a typical metric for characterizing the response of a particle detector. The present work is structured as follows: in Section 2 the experimental setup and procedures are described, Section 3 compiles the scintillation spectra of the pure gases and Ar/CF_4 admixtures; in Section 4 we present a minimalistic kinetic model that describes the observations to good accuracy, and we finally end with a comparison with previous results and a summary of our main conclusions in 5.

2 Experimental setup

Figure 1 shows a schematic drawing of the experimental setup. Measurements were performed on a CF63 aluminum-cube serving as a vessel, irradiated with X-rays from a copper tube at 40 kV. The chamber had an entrance window of 1 cm-diameter made of a thin aluminum foil of 50 μm thickness which was facing the tube. Inside the chamber, an electrifiable cylindrical volume was placed, with 3 cm in diameter and 0.75 cm in height. Its upstream electrode served as a cathode and was made from the same foil as the window. A semitransparent Cr-mesh served as the anode, evaporated on top of a collimating lens (OceanOptics 74-UV) leading to a multi-mode optical fiber (UV-VIS, 600 μm core) and finally coupled to an OceanOptics FX UV-VIS CCD spectrometer sensitive in the 210–800 nm range. The photon spectrometer was calibrated using a lamp with reference light sources for the UV and the visible regions, coupled to the anode mesh. Both calibrations were merged at around the 300 nm mark.

Upon excitation and ionisation of the gas, electrons and ions were collected by means of an uniform electric field, the current being read at the anode with a Keithley picoamperemeter (model 6487). The maximum of the X-ray bremsstrahlung spectrum, when accounting for the absorption in the materials interposed up to the ionization region, was estimated to be at around 12 keV, a

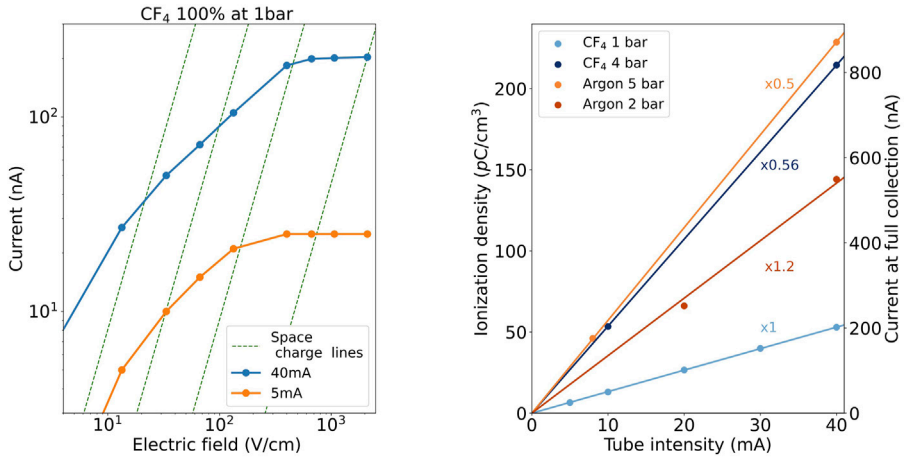

FIGURE 2
Exemplary scans in electric field and X-ray intensity. Left: current at the anode of the scintillation cell as a function of the applied electric field up to reaching full-collection, for different currents of the X-ray tube (pure CF_4 at 1 bar). Green lines represent identical space charge conditions (i.e., same degree of field distortion by positive ions) according to the parameter α introduced in (Palestini and McDonald) and discussed in Section A of the Supplementary Appendix. Right: current at full charge-collection (right axis) and associated ionization density (left axis) calculated using (2.1) as a function of the current of the X-ray tube for CF_4 at 1 and 4 bar (light and dark blue) and pure argon at 2 and 5 bar (red and orange). Each of them was fitted to a proportional trend. (Given the different ion mobility and electrical fields, there is not a global common conversion factor from ionization density to current so each data series includes an additional multiplicative factor in order to transform the right-axis value into the correct one).

characteristic energy for which the X-ray mean free path is 14 cm in argon and 62 cm in CF_4, in standard conditions (Berger et al., 2010). Even for argon at the highest pressures employed in our measurements (5 bar) the mean free path is as large as 2.8 cm, leading to ±10%-level variations within the ionization volume. The size of the ionization cloud (σ) caused by the tortuous trajectory of the ejected photoelectron amounts to about 0.2 cm/P[bar] in argon (see, e.g., Smirnov, 2005; Azevedo et al., 2016), smaller than the chamber dimensions and negligible in the high pressure data. The additional spread stemming from electron diffusion along a 0.75 cm drift-path, when considering electric fields at full charge-collection, can increase the above figure up to 0.16 mm in the radial direction [Pyboltz, (Al Atoum et al., 2020)]. This situation corresponds to pure Ar at 1 bar, with other conditions involving yet smaller charge spreads by roughly a factor of $1/\sqrt{P\,[\mathrm{bar}]}$ as the pressure increases, and up to another factor of ten as CF_4 concentration increases. Overall, inside the collimated region, ionization can be thus regarded as uniform throughout these measurements, for practical purposes.

To exclude space charge and charge-recombination effects, data was taken at no field and at a field high enough to guarantee full charge-collection (Figure 2-left). Along this line, additional measurements were performed for different X-ray intensities too (e.g., Figure 2-right). Under the assumption of uniform irradiation within the collimated region of the scintillation cell (of area $A = \pi^{*}0.5^2$ cm^2), the positive-ion space-charge density ($q_e \cdot dN/dV|_{ion}$) relates to the steady-state current at full collection through:

$$I_{sst} = 2\left(q_e \frac{dN}{dV}\right)_{ion} \cdot A \cdot \mu \cdot E \qquad (2.1)$$

with q_e being the electron charge, μ the ion mobility, E the electric field, and the factor 2 accounts for the equal sharing of current between ions and electrons. The mobilities were evaluated from the ones measured for the Ar^+ ion in Ar in case of pure argon (Walter et al., 2008) and from the ones measured for CF_3^+ in Ar in case of Ar/CF_4 (Santos et al., 2018). Accordingly, the positive-ion space charge ranged in these measurements from 6 pC/cm^3 (for pure CF_4 at around 1 bar and the lowest X-ray intensity) up to 225 pC/cm^3 (for either pure Ar or CF_4 at around 5 bar, and the highest X-ray intensity). At 1 bar these values are about a factor of 4 below those employed in earlier measurements performed under α particles in Morozov et al. (2011), and reported to be recombination-free (see Supplementary Appendix for a detailed comparison). Even the highest pressures explored in this work barely exceed the ionization densities studied earlier, which leads us to believe that recombination is negligible in present conditions. The lack of strong deviations from a proportional behavior in Figure 2-right for different intensities of the X-ray tube adds further support to this.

In order to exclude any space charge effect from the positive ions, the analysis procedure sketched in Palestini and McDonald (2023) was applied. It follows, as discussed in Supplementary Appendix (Section A), that field distortions once the current reached saturation (full collection) were typically at the 5%-level or below (with a maximum field distortion of 15%) during the measurements. The resulting iso-space-charge lines (green dashed, in Figure 2-left) suggest that space charge is the main variable driving the current vs. field behaviour. In the absence of space charge, the extent of fringe fields inside the chamber was evaluated through an axisymmetric finite-element simulation with the COMSOL Multiphysics® package (COMSOL, 2023). As shown in Figure 3-bottom, the electric field is uniform over a region slightly exceeding 2 cm, considerably larger than the size of the ionization volume (collimated down to 1 cm at the chamber entrance -green dashed lines). The values of the electrical potential in 3D, together with the equipotential curves, are shown in Figure 3-top.

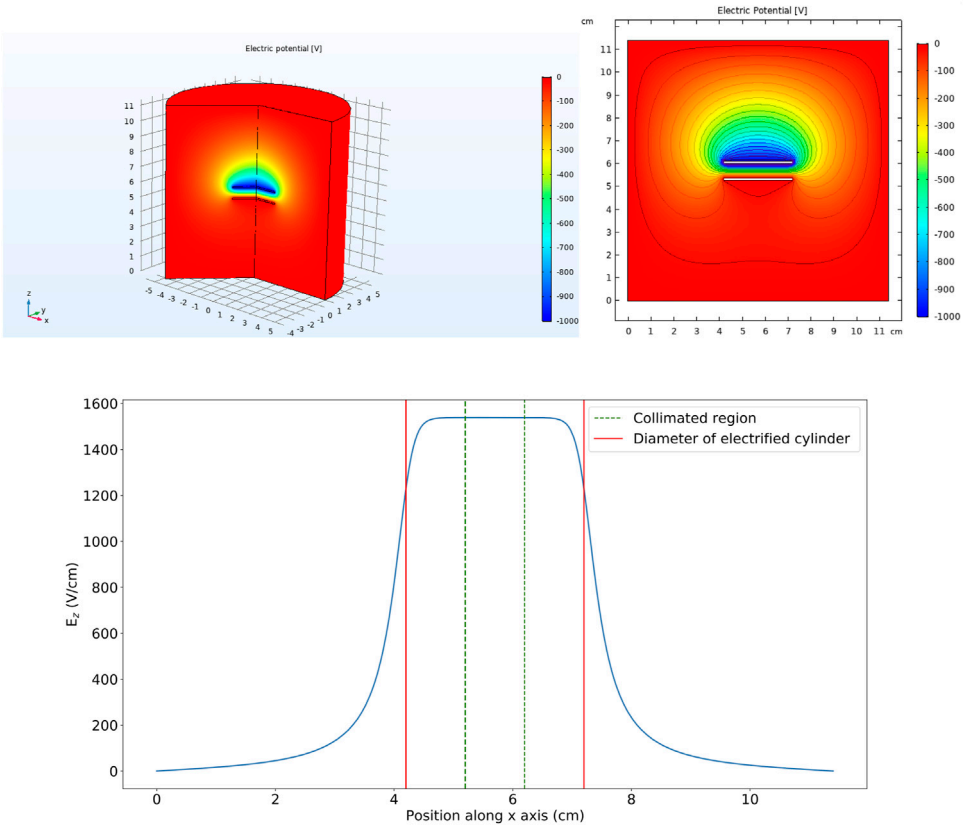

FIGURE 3
Results from an axisymmetric COMSOL simulation, with the X-ray beam impinging from the positive *z*-axis. Top-left: geometry model and electric potential in 3D. Top-right: cross-section at mid-chamber and equipotential curves. Bottom: electric field component perpendicular to the electrodes at mid-chamber (symmetry plane of the cylinder), as a function of the distance from one of the chamber walls.

Prior to the measurements, the chamber was pumped down to 10^{-4} mbar. Ar/CF_4 mixtures were studied at a volume fraction of 100/0, 99.9/0.1, 99.8/0.2, 99.5/0.5, 99/1, 98/2, 95/5, 90/10 and 0/100, and pressures from 1 to 5 bar. The purity of the bottles was 4.5 (CF_4) and 6 (Ar), so the overall purity of the studied mixtures was between 5.5 and 6 (i.e., 1–3 ppm contamination). The chamber was first filled with CF_4 until the desired partial pressure, using two pressure/vacuum gauges, namely, a Pfeiffer Vacuum PCR 280 Pirani/Capacitance and an MKS pressure transducer, for the readings. Afterwards, argon was admixed. Gas circulation was dimmed unnecessary for proper mixing, as the concentration could be verified by sampling the gas into a residual gas analyzer and waiting for the ratio of the pressures of the species to stabilize. This agrees with the notion that the forced flow of argon gas, being dominant by at least a factor 10 in volume, drives the mixing in such a small chamber. For the lowest CF_4 concentrations, that would be limited by the accuracy of the sensor, the filling was done at high pressure and diluted until the target concentration was achieved. Deviations from the target CF_4 concentrations [0, 0.1, 0.2, 0.5, 1, 2, 5, 10, 100]% were quantified through a linear fit and associated uncertainties. Although the target values will be used as plot descriptors in the following, the calibrated values will be used when presenting systematics as well as for model fitting: [0, 0.096 ± 0.015, 0.28 ± 0.024, 0.434 ± 0.026, 0.929 ± 0.071, 1.64 ± 0.14, 5.55 ± 0.21, 10.25 ± 0.39, 100].

Purity was monitored continuously with a residual gas analyzer (RGA) coupled to the main system through a leak valve. The RGA region was kept at a constant pressure of 10^{-5} mbar throughout the measurements by adjusting the leak-valve opening. The main impurities in the system were H_2O, O_2 and N_2(CO) and their concentrations were estimated to be below 1000 H_2O ppm, 15 O_2 ppm and 200 N_2 ppm, being the sensitivity limited by the RGA background. These upper limits, as well as the scintillation yields, showed little variation with time, for a time span of hours. Even if we were to take them as representing the actual concentrations, it has been shown in Margato et al. (2012) that N_2 concentrations as high as 4% are needed to quench CF_4 scintillation by a factor 2 (at 1 bar). Although 1,000 ppms (0.1% per volume) might arguably compete with Ar-CF_4 transfers at about the same CF_4 concentration (the lowest one used in our measurements), the phenomenological model introduced later in text does not show any strong deviation for that case. These observations, together with the nominal purity of the bottles, the use of low-outgassing materials for chamber assembly and the stability of the scintillation yields with time, suggest that the impact of impurities is of little relevance to the results presented in this work.

The final scintillation spectrum was divided by the current at full collection, and by the average energy to create an electron-ion pair (W_I). The latter was taken from the directly-measured values in

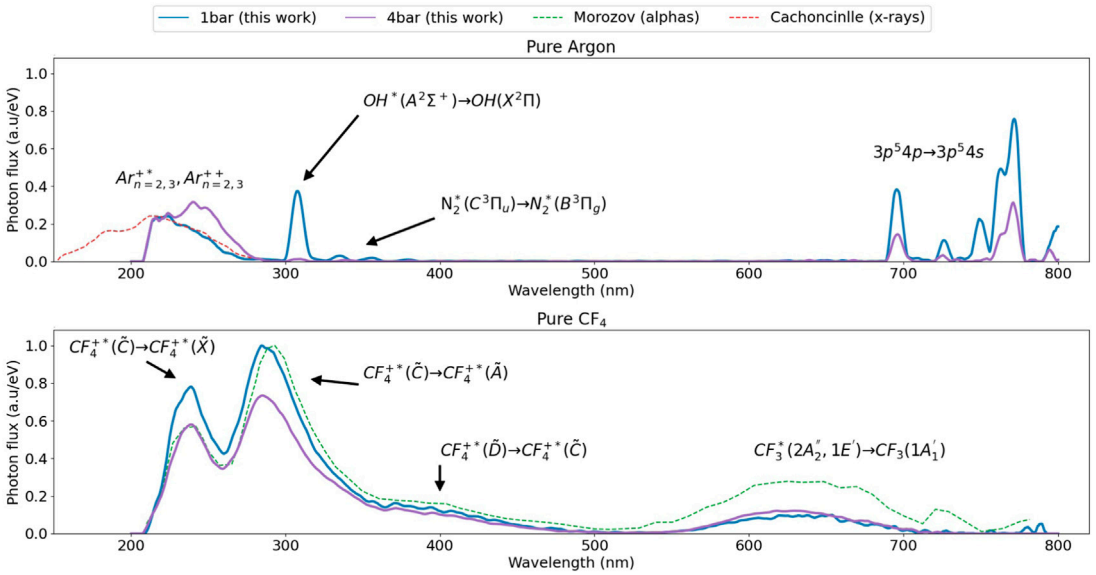

FIGURE 4
Emission spectra per eV of released energy for pure argon (upper plot) and pure CF_4 (lower plot) at 1 and 4 bar (blue, purple), obtained at zero field. No significant dependence with the intensity of the X-ray tube was observed, suggesting that measurements are recombination-free. For pure CF_4, where full charge-collection could be reached before the onset of secondary scintillation, no dependence with the electric field was observed either. The spectra of argon's 3rd continuum obtained in Robert et al. (1995) also with X-rays (red-dashed) and the one of CF_4 obtained in Morozov et al. (2010) with α-particles (green-dashed) are shown for comparison. A global normalization was imposed by setting to 1 the maximum of the 290 nm peak in pure CF_4 at 1 bar.

Reinking et al. (1986), except in the range [0–1]% CF_4 where a simple linear interpolation was used. An absolute normalization was not attempted and thus the spectrum is hereafter expressed in yield/eV [a.u.]. As no significant contribution from recombination or space charge was found in present data, the standard deviation of measurements performed for different X-ray intensities has been used to estimate the uncertainty. This accounts for any residual recombination effect as well as systematic errors that may be present in the measurements.

3 Results

3.1 Pure gases

Figure 4 shows the scintillation spectra of Ar (top) and CF_4 (bottom) at pressures of 1 bar (blue) and 4 bar (purple). The use of arbitrary units (a.u.) makes explicit the absence of absolute normalization, with every spectrum being divided by the total electron current and separately corrected for the average energy to create an electron (W_I), to obtain scintillation yields per eV. Bands that are easily identifiable are the ones of the 3rd continuum of argon (160–280 nm) (Robert et al., 1995) and the (210–500 nm) and (550–750 nm) ones of CF_4 (Morozov et al., 2010). The visible band centered at around 630 nm has been attributed earlier to the transition $CF_3^*(2A_2'', 1E') \rightarrow CF_3(1A_1')$ (Suto et al., 1983; Washida et al., 1983; Lee et al., 1986) (not being assigned unequivocally to either the $2A_2''$ or the $1E'$ states). The overlapping UV bands can be attributed to the $CF_4^{+,*}$ ion, emitting from its $\tilde{C}, \tilde{D}$ states. Transitions $\tilde{C} \rightarrow \tilde{X}, \tilde{A}$ can be naturally assigned to the peaks centered around 230 nm and 290 nm (Harshbarger et al., 1972; Lambert et al., 1988; Zhang et al., 1989) while the transition at 364 nm may be assigned to $\tilde{D} \rightarrow \tilde{C}$. Another prominent UV band at around 260 nm has been observed before, e.g., under excitation within low-energy electron avalanches (Fraga et al., 2003), and can be assigned to the transition $CF_3^*(2A_1') \rightarrow CF_3(1A_2'')$ (Washida et al., 1983; Lee et al., 1986); it is however hidden in present conditions under the $CF_4^{+,*}$ emission. The small decrease of the yields in the UV bands as a function of pressure has been observed before in Morozov et al. (2010) and might be naturally attributed to self-quenching. A comparison with data from Morozov et al. (2010) obtained at 1 bar under α-particle irradiation is shown in Figure 4 (green, dashed), arbitrarily normalized to the 290 nm peak.

Concerning Ar, the 3rd continuum (cut by the spectrometer bandwidth below 210 nm) agrees in shape with earlier X-ray measurements from Robert et al. (1995), increasing the yield on its blue-wing as the pressure increases, qualitatively in agreement with that work too (red dashed-line). In the near-infrared region the main lines located at 696, 727, 750, 763 and 772 nm can be clearly identified, corresponding to transitions between the $3p^54p$ and $3p^54s$ multiplets (Reader et al., 1980). Their associated yields seem to be dominated by 2-body collisional self-quenching, thus approximately following a $\sim 1/(a + bP)$ trend, except in the case of the 750 nm peak where a $\sim 1/(a + bP^2)$ trend is observed instead (Figure 5). The strong suppression observed as a function of CF_4 concentration suggests that argon IR-yields will be subdominant in high pressure applications and/or as soon as a molecular additive is added.

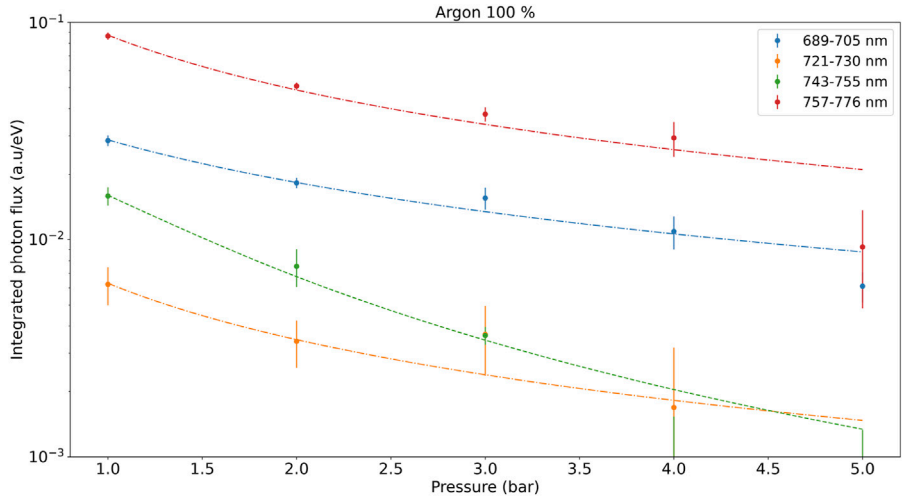

FIGURE 5
Integrated yields for different argon near-infrared peaks as a function of pressure. Dashed-dotted lines represent a fit to a 2-body self-quenching law while the dashed-green line follows from three-body self-quenching.

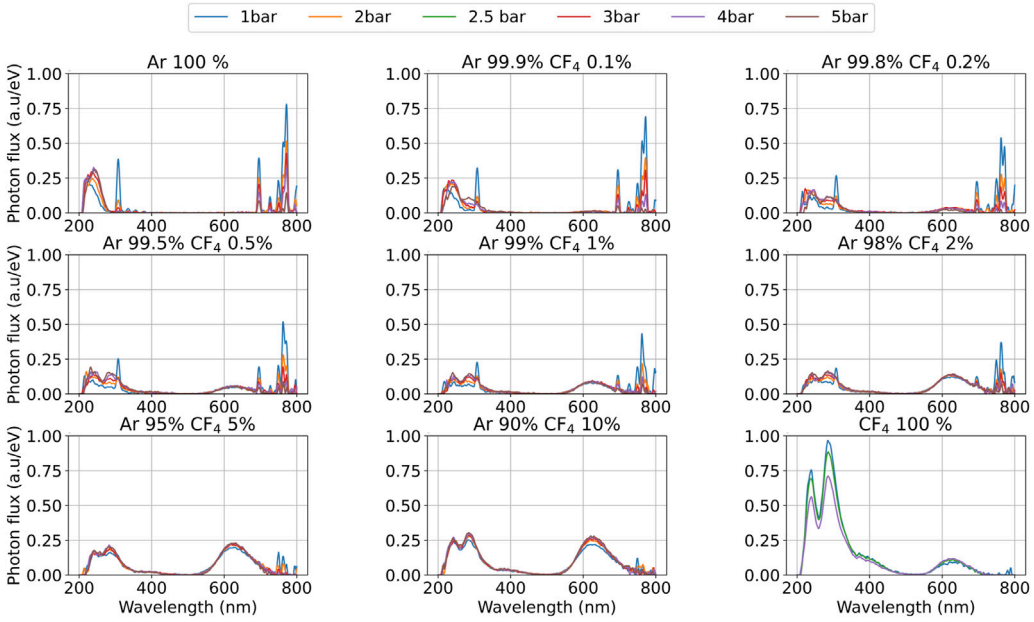

FIGURE 6
Emission spectra per eV of released energy for different concentrations of Ar/CF_4, at zero field. Measurements are expected to be free from recombination effects, as discussed in text. A global normalization was imposed by setting to 1 the maximum of the 290 nm peak in pure CF_4 at 1 bar. The exact CF_4 concentrations (after calibration) can be found in Figure 13 in (Supplementary Appendix C).

The presence of impurities can be derived from the peak at around 310 nm, corresponding to the $OH^*(A^2\Sigma^+) \rightarrow OH(X^2\Pi)$ transition (Müller et al., 1993; Maslaáni and Sember, 2014). It can be attributed to charge transfer between Ar^+ and H_2O^+, following dissociative recombination to populate OH^* (Maslaáni and Sember, 2014). Even if barely visible, N_2 peaks at around 335, 355 and 380 nm are present in argon too, as expected from the transfer reactions identified in Takahashi et al. (1983).

3.2 Ar/CF_4 mixtures

Figure 6 compiles the spectra for different Ar/CF_4 admixtures and pressures. Although they were obtained at zero field, no significant dependence with the X-ray intensity or electric field was observed, demonstrating the absence of recombination effects. This was generally the case except below 1% CF_4, conditions for which the energy of the ionization electrons is high enough to cause neutral bremsstrahlung radiation (NBrS)

during their drift (Buzulutskov et al., 2018; Amedo et al., 2022; Henriques et al., 2022) at the fields required for full charge-collection, thus complicating the interpretation. Exemplary, for the full-collection field of 2900 V/cm in pure Ar at 1 bar, NBrS would amount to about ~ 0.015 ph/eV in the region 210–800 nm (Amedo et al., 2022). Given its flat nature, NBrS easily overwhelms the 3rd continuum in the region around 200–350 nm, if assuming that the integral of the latter amounts to 0.0036 ph/eV, as recently measured in Santorelli et al. (2021). These results are not presented here as they will be discussed in detail elsewhere.

Indirectly, the low impact of recombination light in the window 210–800 nm for low CF_4 concentrations may be inferred from: i) its absence for mixtures above 1% CF_4 (e.g., Supplementary Figure SA12 in Supplementary Appendix) for which the ionization densities are similar; ii) the fact that full charge-collection is reached to within less than 5% for all conditions (e.g., Figure 2); iii) the fact that NBrS constitutes a featureless continuum above a certain wavelength threshold depending on the electron energy (Henriques et al., 2022) and, within that assumption, no significant field-induced modification of the characteristic UV and visible bands of the Ar/CF_4 scintillation could be observed below 1% CF_4.

In the spectra shown in Figure 6 it can be seen that the transition between the pure-argon spectrum and the CF_4 one starts to happen as soon as 0.1% CF_4 is introduced. At that concentration, the appearance of a new peak at 290 nm and the small bump at around the CF_3^* band hint towards a contribution beyond that of direct CF_4 excitation, that would be otherwise suppressed 1,000 times relative to the 100% CF_4 case. The 3rd continuum from argon quenches rapidly as CF_4 increases and it halves for just 0.2% CF_4. For higher concentrations, the appearance of the $CF_4^{+,*}$ band associated to the $\tilde{C} \rightarrow \tilde{X}$ transition (centered at 230 nm) obscures the effect. As already noted, the near-infrared emission from argon displays self-quenching as the pressure increases, but it is also strongly suppressed in the presence of CF_4, becoming undetectable above 5% CF_4 at 5 bar. The N_2 bands resulting from Ar* transfers disappear already at 0.1% CF_4, suggesting that N_2 contamination is well below that concentration, if recalling that the Ar* quenching rates are comparable for the two molecules (Velazco et al., 1978). The most prominent contamination in the system seems to be H_2O, that leads to OH* emission at around 310 nm and is arguably driven by $Ar^+ + H_2O \rightarrow Ar + H_2O^+$ charge transfer (Maslaáni and Sember, 2014). Given the shape-modification observed for the UV band of CF_4 at around 1 bar (where the presence of the OH* peak is most prominent relative to higher pressures), it cannot be fully excluded that H_2O might have a small influence in that case, specially for low CF_4 concentrations. For high pressures and high CF_4 concentrations, the OH* peak vanishes and the UV spectra stabilizes. Collisional-relaxation of $CF_4^{+,*}(v)$ sates down to the bottom of the potential well $CF_4^{+,*}(v = 0)$ represents a plausible alternative, that would also explain the emergence of fully-formed UV bands when pressure and CF_4 concentration increases (as Ar is *a priori* inefficient for this process).

Figure 7 compiles the integrated yields in the most representative regions (210–250 nm, 250–350 nm, 350–400 nm and 400–700 nm) for different pressures and as a function of the CF_4 concentration. The trend of the 210–250 nm emission (blue) follows from the quenching of the Ar 3rd continuum, with $CF_4^{+,*}$ emission from $\tilde{C} \rightarrow \tilde{X}$ taking over as the CF_4 concentration increases, causing a minimum for concentrations around 1% CF_4. In the other UV bands the increase is monotonous with CF_4 while the visible band shows an optimum for concentrations around or above the ones studied in this work. In general, visible-range yields are significantly increased over the ones in pure CF_4 in the range 2%–10%, and can be anticipated beyond the upper concentration studied in this work. A kinetic model addressing the observed behaviour is sketched in the next section.

4 Discussion

4.1 Wavelength-shifting pathways

Our data presents strong evidence of wavelength-shifting and in particular Figure 7 suggests, qualitatively, that scintillation in the 630 nm band (CF_3^*) must feed from Ar* transfers and not just through direct CF_3^* formation, otherwise a proportional trend would be expected. The observed increase (approximately proportional up to 1%CF_4) shows a drop above or around 10%CF_4 and might still be attributed to direct CF_3^* formation followed by self-quenching with CF_4. However this would imply a strong dependence with pressure, that is not seen in data. Figure 8 shows for illustration a spectral comparison with the CF_4 and He/CF_4 systems, for which the CF_3^* band appears depopulated relative to the UV one, adding further support to the role of Ar* states at CF_3^* formation. Given that the threshold for CF_3 production sits at 12.5 eV (Winters and Inokuti, 1982) and the one for CF_3^+ production at around 16 eV (Zhang et al., 1989; Christophorou et al., 1996), the threshold for CF_3^* production must lie in between. This indicates that the Ar* state(s) involved in transfers lie well above the lowest-lying Ar excited states at 11.5 eV and close to the continuum (IP_{Ar} = 15.7 eV), thereby labeled Ar** hereafter. A discussion on the nature of such a state(s) is postponed to the end of this section. On the other hand, the UV scintillation may be tentatively attributed to transfers involving the higher-lying 3rd continuum precursors ($Ar_{n=2,3}^{*,+}$, $Ar_{n=2,3}^{++}$) (Wieser et al., 2000). The fact that the yields in the region 210–250 nm and 250–350 nm show opposing trends up to around 1% CF_4, with the total yield remaining approximately constant, is a good indicator that the energy is being transferred between species. The extracted quenching rates and spectral shapes add further support to this interpretation, as shown later.

A kinetic model has been developed keeping the above considerations in mind, in order to quantitatively interpret our experimental results. It is sketched in Figure 9 and detailed in the following.

Aiming at a reduced number of model parameters, the 3rd continuum precursors are characterized through an effective decay constant of 5 ns (e.g., Santorelli et al., 2021):

$$Ar_{n=2,3}^{+,*}, Ar_{n=2,3}^{++} \xrightarrow{\tau_{3rd}} Ar^+ + Ar^{(+)}(+Ar) + h\nu(180 - 300\,nm) \quad (4.1)$$

For CF_4, the states that leave a clear footprint in the spectra can be matched to the following decays:

$$CF_3^*(2A_2'', 1E') \xrightarrow{\tau_{CF_3}} CF_3(1A_1') + h\nu(630\,nm) \quad (4.2)$$

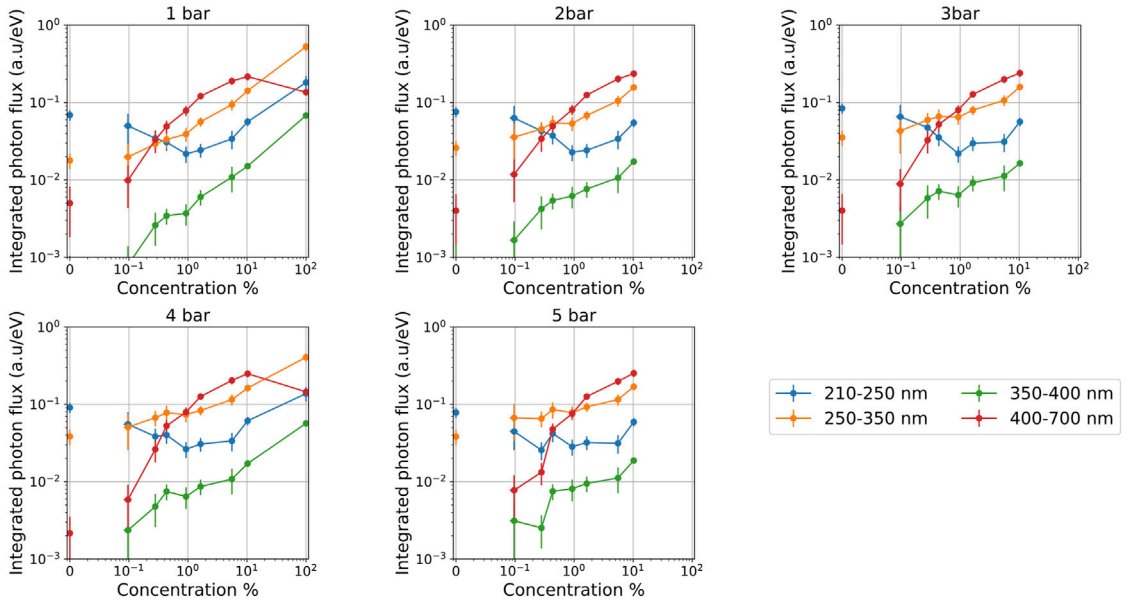

FIGURE 7
Integrated scintillation yields for the Ar/CF_4 system (per eV of released energy), shown in different bands as a function of CF_4 concentration, for different pressures. Zero-concentration yields have been added to the logarithmic *x*-axis to illustrate the asymptotic behaviour. (The argon peak located at 700 nm and the peaks caused by impurities were removed from this analysis; measurements on pure CF_4 were only carried out at 1 and 4 bar; yields below 10^{-3} are not shown as the uncertainty bar is larger than 100%).

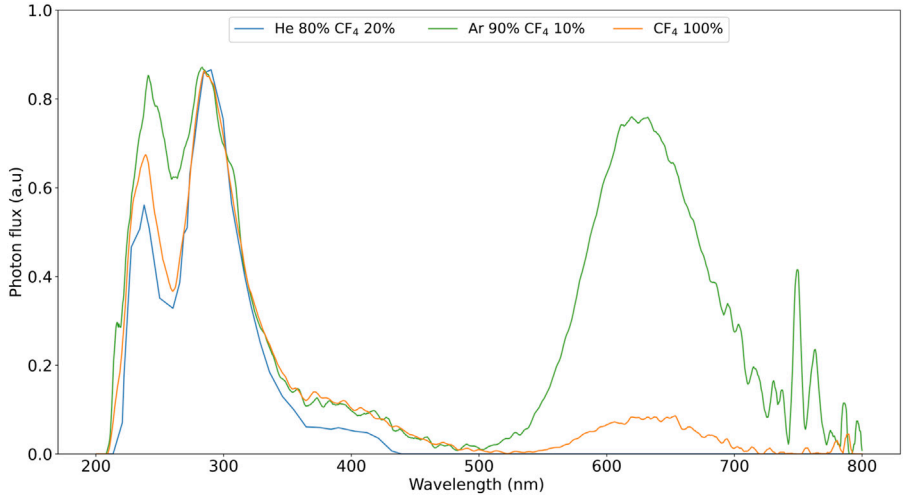

FIGURE 8
Comparison between the primary scintillation spectrum for pure CF_4 (orange), Ar/CF_4 at 10% per volume (green) and He/CF_4 at 20% per volume (blue), at 1 bar. All spectra have been arbitrarily normalized to the 290 nm UV peak.

$$CF_4^{+,\star}\left(\tilde{C}\right) \xrightarrow{\tau_{CF_4(C->X)}} CF_4^{+}\left(\tilde{X}\right) + h\nu(230\,nm) \quad (4.3)$$

$$CF_4^{+,\star}\left(\tilde{C}\right) \xrightarrow{\tau_{CF_4(C->A)}} CF_4^{+,\star}\left(\tilde{A}\right) + h\nu(290\,nm) \quad (4.4)$$

To the best of our knowledge, not all the possible decays of the accessible $CF_4^{+,\star}$ states have been observed in literature, e.g., $CF_4^{+,\star}$ (B) → $CF_4^{+,\star}$ (A). As $CF_4^{+,\star}$ states are unstable (Zhang et al., 1989), it is possible that dissociation out-competes radiative decay in some of them. For the states involved in Eqs 4.2–4.4, however, we opted to assign a decay probability of 100% to avoid the introduction of new additional parameters. As shown later, a good χ^2 is obtained in the proposed kinetic scheme through a global fit employing two parameters per spectral region (UV and visible), so a further increase in the number of parameters was deemed unnecessary.

Transfer reactions between Ar states and CF_4 represent the last ingredient. For the visible component, we make the natural assumption that transfers between the Ar** state(s) and CF_4 compete just with self-quenching, summarized as:

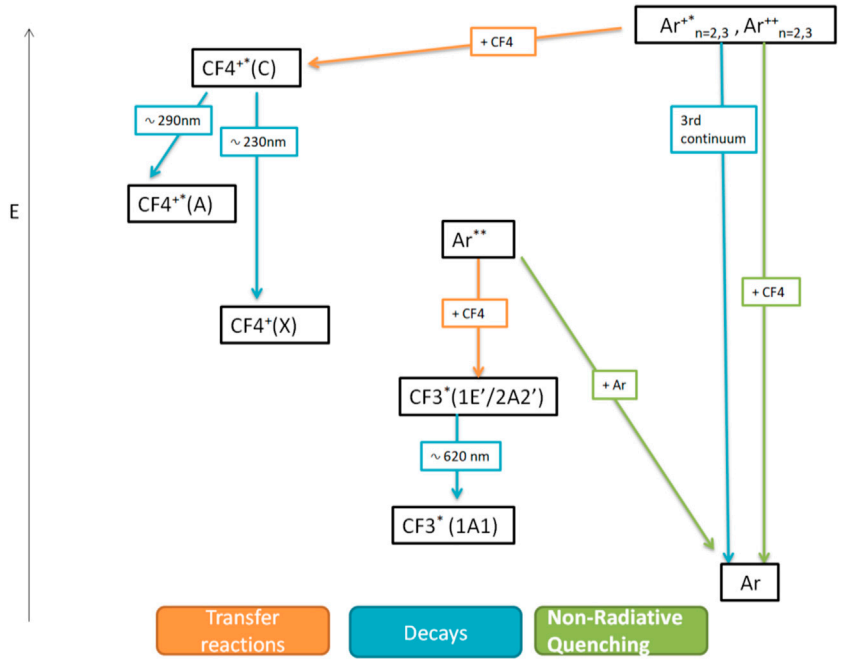

FIGURE 9
Kinetic scheme used to describe wavelength-shifting in Ar/CF_4 mixtures. The main scintillation drivers are the $CF_4^{+,*}$, CF_3^* and Ar 3rd continuum states. Energy considerations lead to the hypothesis of an additional high-lying Ar** state, whose nature is discussed in text.

$$Ar^{**} + CF_4 \xrightarrow{k_{Ar^{**}->CF_3^*}} Ar + CF_3^*(2A_2'', 1E') \tag{4.5}$$

$$Ar^{**} + Ar \xrightarrow{k_{Ar^{**}->Ar^*}} Ar^* + Ar \tag{4.6}$$

It is in principle possible to include an additional non-radiative quenching channel of Ar** with CF_4, that has been neglected again on the basis that it is not needed to describe data and it would add unnecessary complexity to the model. Within the proposed kinetic scheme, Ar** transfers would lead to CF_3^* scintillation with near-100% probability.

Last, we consider transfer reactions leading to UV emission between the 3rd continuum precursors and CF_4, together with a quenching reaction to non-radiative states:

$$Ar_{n=2,3}^{+,*}\left(Ar_{n=2,3}^{++}\right) + CF_4 \xrightarrow{k_{Ar^{3rd}->CF_4^{+,*}}} Ar + CF_4^{+,*}\left(\tilde{C}\right) \tag{4.7}$$

$$Ar_{n=2,3}^{+,*}\left(Ar_{n=2,3}^{++}\right) + CF_4 \xrightarrow{k_{Ar^{3rd}->Ar}} \text{non} - \text{radiative} \tag{4.8}$$

where rates for transfer and non-radiative quenching have been introduced for an "effective" 3rd continuum precursor. Along this line, reactions of 3rd continuum states with ground-state Ar are assumed to be already accounted for when considering the kinetics of such an "effective" precursor, and remain unaltered in the presence of CF_4 [for a detailed pathway scheme of the 3rd continuum formation, the reader is referred to Wieser et al. (2000)]. In the following, reaction rates [t^{-1}] are defined for 1 bar of the reactive, and scaled based on pressure and species concentration [as done for instance in Azevedo et al. (2018)].

Before evaluating the model, it should be noted that the possibility of self-quenching of the $CF_3^*(2A_2'', 1E')$ state with CF_4 has been omitted due to the negligible pressure-dependence of Ar/CF_4 scintillation in the 630 nm band. $CF_4^{+,*}$ states, on the other hand, evidence a small self-quenching on the UV region in pure CF_4, compounded with the aforementioned indications of collisional relaxation for Ar/CF_4 mixtures at low pressures and CF_4 concentrations. Such dependences with pressure can be easily included in the model but, being a small effect and not shedding light into the main transfer mechanisms, they have been omitted for the sake of simplicity. The near-visible band centered around 364 nm, arising from the $\tilde{D} \rightarrow \tilde{C}$ transition, is also not considered given its relatively small contribution to the total spectrum.

From the above set of reactions 4.1–4.8 it is possible to derive the scintillation probability (per eV of energy deposited in the medium) of the states $CF_3(2A_2'', 1E')$, $CF_4^{+,*}(\tilde{C})$, and of the effective state Ar^{3rd}:

$$P_{\gamma,CF_3^*} = f_{CF_4} \cdot P_{\gamma,CF_3^*}\big|_{dir} + \left((1 - f_{CF_4}) \cdot P_{Ar^{**}} \cdot \frac{K_{Ar^{**}->CF_3^*}}{K_{Ar^{**}->CF_3^*} + \frac{(1 - f_{CF_4})}{f_{CF_4}} \cdot K_{Ar^{**}->Ar^*}} \right) \tag{4.9}$$

$$P_{\gamma,CF_4^{+,*}} = f_{CF_4} \cdot P_{\gamma,CF_4^{+,*}}\big|_{dir} + \left((1 - f_{CF_4}) \cdot P_{Ar^{3rd}} \cdot \frac{f_{CF_4} \cdot n \cdot K_{Ar^{3rd}->CF_4^{+,*}}}{1/\tau_{3rd} + f_{CF_4} \cdot n \cdot \left(K_{Ar^{3rd}->CF_4^{+,*}} + K_{Ar^{3rd}->Ar}\right)} \right) \tag{4.10}$$

$$P_{\gamma,Ar^{3rd}} = (1 - f_{CF_4}) \cdot P_{Ar^{3rd}} \cdot \left(\frac{1/\tau_{3rd}}{1/\tau_{3rd} + f_{CF_4} \cdot n \cdot \left(K_{Ar^{3rd}->CF_4^{+,*}} + K_{Ar^{3rd}->Ar}\right)} \right) \tag{4.11}$$

Here f_{CF_4} represents the CF_4 concentration, n equals the pressure ratio P/P_0, and the quenching and transfer rates are the ones defined

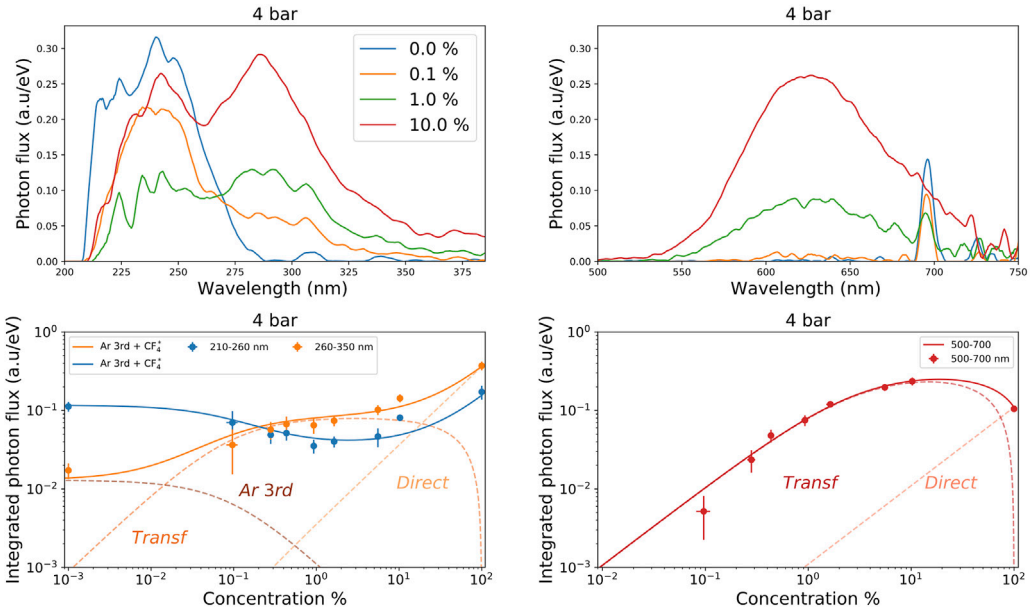

FIGURE 10
Top row: scintillation spectra for different CF_4 concentrations at 4 bar, zoomed in the ultraviolet (left) and visible (right) regions. Bottom row: integrated yields on the ultraviolet (left) and visible (right) regions (shown as closed circles), superimposed to the kinetic model introduced in text. The experimental value for zero concentration is added on the bottom-left plot at 0.001% CF_4, taking advantage of the fact that the model asymptotically tends to a constant in that case.

in Eqs 4.5–4.8. Parameters with subscript 'dir' refer to the probability of direct scintillation, and $P_{Ar^{**}}$, $P_{Ar^{3rd}}$ stand for the formation probability of the Ar** state(s) and of the 3rd continuum precursors, respectively. Some of the parameters needed to evaluate the above equations can be constrained based on existing experimental data, including this work. The direct scintillation probabilities, for instance, as well as the probability of formation of 3rd continuum precursors, can be obtained from the yields in pure CF_4 and pure argon. The time constant for the argon 3rd continuum has been taken from Santorelli et al. (2021). Further, based on the model structure, only the ratio of Ar** transfer to quenching rates in Eq. 4.9 is relevant, reducing the total number of fit parameters to four. The other three parameters represent the formation probability of Ar** states, and the non-radiative quenching and transfer rates of $CF_4^{+,*}$. The model structure also makes explicit the lack of pressure-dependence of CF_3^* scintillation observed for any admixture.

A weighted global fit of the proposed kinetic model to the three data series associated with the 230, 290 and 630 nm bands was performed. Yields in the first two bands were fitted to a sum of Eqs 4.10, 4.11 and the 630 nm band was described through Eq. 4.9. The fit is shown in Figure 10 for a pressure of 4 bar (blue, orange, red lines), alongside the corresponding experimental data (full circles). Its reduced χ^2 of 1.56 adds plausibility to the present interpretation. The following values and uncertainties were obtained for the fit parameters: $P_{Ar^{**}}/P_{Ar^{3rd}} = 3.19 \pm 0.39$ (population of Ar** relative to that of 3rd continuum precursors); $\frac{K_{Ar^{**}->CF_3^*}}{K_{Ar^{**}->Ar^*}} = 36.5 \pm 7.9$ (ratio of transfer to collisional quenching of Ar**); $K_{Ar^{3rd}->CF_4^{+,*}} = 49 \pm 18$ ns^{-1} (transfer rate of the Ar 3rd continuum) and $K_{Ar^{3rd}->Ar} = 4.1 \pm 3.3$ ns^{-1} (non-radiative quenching rate of the Ar 3rd continuum). Within the proposed kinetic model, the ratio of transfer-mediated scintillation to direct scintillation can be computed: for 1% CF_4, illustratively, values as large as 72 ± 20 (visible) and 20.9 ± 2.1 (UV) are obtained.

In the UV-band, a detailed analysis of the spectral shapes (Figure 10 top-left) brings additional support to the proposed interpretation: as soon as 0.1% CF_4 is added to argon, there is a strong suppression of the argon 3rd continuum, coinciding with the appearance of the 290 nm peak from $CF_4^{+,*}$. For 1% CF_4, the effect is even more clear. Taking as a reference the yields measured earlier for α-particles in the Ar 3rd continuum [around 3,500 ph/MeV (Santorelli et al., 2021)] and in the VUV-visible range of CF_4 [1,000–3,000 ph/MeV (Pansky et al., 1995; Azmoun et al., 2010; Morozov et al., 2010; Lehaut et al., 2015)], it is implausible that direct CF_4 excitation could be responsible for the observed levels of X-ray scintillation when the species is present at a mere sub-percent level. Above 1% CF_4, the overlap between argon 3rd continuum and the $CF_4^{+,*}$ emission at 230 nm complicates a qualitative description, and a direct comparison with the proposed kinetic model has to be used instead (Figure 10 bottom-left). In any case, the fact that the number of photons emitted in the UV region is maintained approximately constant when transfer reactions dominate (i.e., below a few % CF_4) reinforces the idea that the kinetics of the Ar 3rd continuum states drives the UV scintillation of the admixture, and that the $CF_4^{+,*}$ state scintillates efficiently upon transfer, as assumed. Although the agreement seems convincing, additional support to the proposed pathway scheme can be found: according to the model, the scintillation of the argon 3rd continuum gets quenched down to just 8.6% ± 2.8% of its nominal value in the pure gas when in presence of 1% CF_4. This is compatible with the quenching level that has been reported for the Ar 3rd continuum when admixed with CO_2, at about 1% concentration (Strickler and Arakawa, 1964).

Given that both CF_4 and CO_2 are energetically accessible to transfers from the high-lying $Ar^{\ddagger}_{2,3}$ and $Ar^{++}_{2,3}$ states, and the similar molecule size, this approximate agreement is reassuring.

In the visible band, the proposed model where CF_3^* formation competes with self-quenching provides a natural explanation for the total absence of pressure dependencies. It requires, however, the somewhat artificial introduction of a new Ar** state or set of states. Invoking the 3rd continuum precursors cannot be excluded, although it would require increasing the model complexity substantially: the behaviour of the transfer reactions involved in UV and visible scintillation (Figure 10-bottom) is too different to be easily attributable to the same state. As discussed earlier, the existence of Ar** states is justified by energy considerations, given that they must be several eV above the Ar* 2nd continuum precursors at around 11.5 eV, yet below the argon IP (15.7 eV) in order to induce excited dissociation of CF_3^*. According to our model, the formation probability of Ar** is about × 3 that of Ar^{3rd} states, that would imply [if using for reference the 2nd and 3rd continuum yields measured in Santorelli et al. (2021)] a substantial part of the available Ar excited states being eligible for transfer (about 50%). Also, the transfer rate would need to be nearly 40 times larger than self-quenching with Ar (36.5 ± 7.9 from our fit) and it remains open which mechanism could cause such large transfer values. Although the role of the Ar** states cannot be excluded from present results, there is an alternative explanation in the formation of an $ArCF_3^*$ exciplex. There is apparently no information in literature about this process that is, e.g., generally absent in the modelling of Ar/CF_4 discharges (Bi et al., 2009; Bai et al., 2018; Toneli et al., 2019). $ArCF_3$ is iso-electronic with CF_4^- that is in fact known not to be stable, except in the presence of $(CF_4)_n$ clustering (Gutsev and Adamowicz, 1995). There are suggestions of the formation of the (expectedly more stable) CF_4^{-*} state in some works (e.g., Kumar et al., 2008), but not enough evidence is provided. If the binding energy of such an exciplex would be on the order of few eV, it is conceivable that it could be formed starting from the long-lived Ar_2^* triplet state. Although speculative at the moment, such a mechanism would provide a natural explanation for the lack of pressure-dependence, the similarity between the populations of Ar** and 2nd continuum precursors, as well as for the preponderance of wls-transfers in Ar compared to, e.g., He.

4.2 Comparison with previous results

The results obtained in this work may be compared with the ones obtained for Ar/CF_4 mixtures in a 9 MeV proton beam at 1 bar in Liu et al. (2012). Little details are found there in regard to space charge, recombination and beam-induced scintillation and in fact the relative normalization of the visible/UV bands is not given either. Qualitatively, it is possible to see that the relative increase in both the visible and UV bands from 1% to 10% CF_4 concentrations is around a factor 3, compatible with present results. The region above 700 nm is characterized by the presence of an additional molecular emission while the Ar IR emission appears fully quenched, both observations being in stark contrast with our results. The absence of data for pure CF_4 together with the strong contamination found for argon data in that work, preclude any estimate of the photon yields or wavelength-shifting capability.

A spectral comparison between scintillation induced by X-rays (this work) and α-particles [in Morozov et al. (2010)] seems more reliable at this point, and can be seen in Figure 4 (green, dashed). Both spectra were obtained at 1 bar, arbitrarily normalized to the 290 nm peak. They display an approximate agreement in the UV and blue regions, however the emission in the red region appears off by a factor of 2.8. The discrepancy is preserved when considering the ratio between the other two UV peaks and the $CF_3^*(2A_2'', 1E') \rightarrow CF_3(1A_1')$ one at 630 nm. These transitions are well above the calibration mark of the lamp at 300 nm and also far enough into the visible region so that we can safely exclude any strong wavelength-asymmetry of the light collection process in the chamber compared to the calibration setup. As no hints of charge recombination were observed at 1 bar neither in Morozov et al. (2010) nor in this work, these measurements point to a fundamental difference between the scintillation mechanisms for α particles and X-rays in CF_4.

Last, it must be recalled that the strength of CF_4 scintillation in the VUV-visible range, as obtained for α particles at 1 bar, is currently found at levels of 1,000–3,000 ph/MeV (Pansky et al., 1995; Azmoun et al., 2010; Morozov et al., 2010; Lehaut et al., 2015). Values within this range have been reported, too, for Ar/CF_4 mixtures around 10 bar in Amedo (2021). Nonetheless, the large experimental spread on the above CF_4 yields, together with the particle-dependence of the spectral emission reported here, call for future studies on the scintillation yields of these type of mixtures.

5 Conclusion

We have presented a comprehensive data-set on the primary scintillation spectra of Ar/CF_4 mixtures in the pressure range 1–5 bar and CF_4 concentrations from 0.1% to 10%, including pure gases. Our results, obtained under strong X-ray irradiation yet in conditions shown to be free from recombination and space charge effects, provide a clear indication that Ar 3rd-continuum precursors play a pivotal role in the UV-scintillation of Ar/CF_4 mixtures. On the other hand, a high-laying Ar** state or an $ArCF_3^*$ exciplex seem the most plausible candidates leading to CF_3^* formation (responsible for the scintillation in the visible range), with a simple pathway scheme explaining the observed phenomenology, in particular the lack of pressure-dependence of the measured yields. The proposed kinetic model resorts to just four parameters (two per emission band), achieving a satisfactory agreement with a reduced χ^2 of 1.56. A more complex mechanism starting from the precursors of the Ar 3rd continuum could still be advocated to cause scintillation in the visible range, however its elucidation does not seem accessible to present experimental conditions.

In sum, wavelength-shifting in the Ar/CF_4 system is very strong for the conditions studied: at a mere 2% CF_4, for instance, scintillation in the 500–700 nm (CF_3^*) band exceeds that of pure CF_4 with independence from pressure. UV scintillation remains at strengths comparable to the visible one in the concentration range 1%–10% CF_4, and progressively dominates outside it. Overall, upon

just 1% CF_4 addition, the ratio of transfer-mediated scintillation to direct scintillation is estimated to be as large as 72 ± 20 (visible) and 20.9 ± 2.1 (UV).

Our measurements convey as well strong evidence of the dependence of the spectra of emission on particle type. The ratio of the UV/visible bands, as observed for X-rays in this work, is about × 2.8 larger than measured earlier for α's in pure CF_4 at around 1 bar, both performed in recombination-free conditions. Overall, the presented results show great promise for technological applications in future particle detectors in the fields of rare event searches, nuclear and neutrino physics.

Data availability statement

The original contributions presented in the study are included in the article/Supplementary Material, further inquiries can be directed to the corresponding author.

Author contributions

PA: Conceptualization, Data curation, Formal Analysis, Investigation, Methodology, Software, Writing–original draft, Writing–review and editing. DG-D: Conceptualization, Funding acquisition, Investigation, Methodology, Resources, Supervision, Writing–original draft, Writing–review and editing. FB: Conceptualization, Investigation, Methodology, Supervision, Writing–review and editing. DF-P: Software, Visualization, Writing–review and editing. EO: Conceptualization, Funding acquisition, Project administration, Resources, Writing–review and editing. LR: Conceptualization, Funding acquisition, Project administration, Resources, Writing–review and editing.

Funding

The author(s) declare financial support was received for the research, authorship, and/or publication of this article. This research was funded by the Spanish Ministry ("Proyectos de Generación de Conocimiento," PID 2021-125028OB-C21), Xunta de Galicia (Centro singular de investigación de Galicia, accreditation 2019-2022), and by the "María de Maeztu" Units of Excellence program MDM 2016-0692. DGD was supported by the Ramón y Cajal program (Spain) under contract number RYC-2015-18820.

Acknowledgments

The authors want to thank Saulo Vázquez (USC) for his valuable insights on the chemistry of Ar/CF_4 reactions and L. Margato (LIP-Coimbra) for useful feedback.

Conflict of interest

The authors declare that the research was conducted in the absence of any commercial or financial relationships that could be construed as a potential conflict of interest.

The authors GD-G and FB declared that they were editorial board members of Frontiers, at the time of submission. This had no impact on the peer review process and the final decision.

Publisher's note

Supplementary material

The Supplementary Material for this article can be found online at: http://www.frontiersin.org/articles/10.3389/fdest.2023.1282854/full#supplementary-material

References

Abed Abud, A., Abi, B., Acciarri, R., Acero, M. A., Adamov, G., Adams, D., et al. (2023). *DUNE collaboration), A gaseous argon-based near detector to enhance the physics capabilities of DUNE*, 06281v1. arXiv:2203.

Abi, B., Acciarri, R., Acero, M., Adamov, G., Adams, D., Adinolfi, M., et al. (2020). Volume I. Introduction to DUNE. *JINST* 15, T08008. doi:10.1088/1748-0221/15/08/t08008

Al Atoum, B., Biagi, S. F., González-Díaz, D., Jones, B. J. P., and McDonald, A. D. (2020). Electron transport in gaseous detectors with a python-based Monte Carlo simulation code. *Comput. Phys. Commun.* 254, 107357. doi:10.1016/j.cpc.2020.107357

Amedo, P., Leardini, S., Saá-Hernández, A., and González-Díaz, D. (2021). Primary scintillation yields of α particles in pressurized Argon-CF_4 mixtures, in preparation, Preliminary results in LIDINE 2021. https://indico.physics.ucsd.edu/event/1/contributions/62/.

Amedo, P., González-Díaz, D., and Jones, B. J. P. (2022). Neutral bremsstrahlung in TPCs. *J. Instrum.* 17, C02017. doi:10.1088/1748-0221/17/02/c02017

Araújo, H. M., Balashov, S., Borg, J., Brunbauer, F., Cazzaniga, C., Frost, C., et al. (2023). The MIGDAL experiment: measuring a rare atomic process to aid the search for dark matter. *Astropart. Phys.* 151, 102853. doi:10.1016/j.astropartphys.2023.102853

Azevedo, C. D. R., González-Díaz, D., Biagi, S., Oliveira, C., Henriques, C., Escada, J., et al. (2018). Microscopic simulation of xenon-based optical TPCs in the presence of molecular additives. *Nucl. Instrum. Methods Phys. Res. Sect. A Accel. Spectrom. Detect. Assoc. Equip.* 877, 157–172. doi:10.1016/j.nima.2017.08.049

Azevedo, C. D. R., González-Díaz, D., Correia, P., Biagi, S., Silva, A., Carramate, L., et al. (2016). Pressure effects on the X-ray intrinsic position resolution in noble gases and mixtures. *J. Instrum.* 11 (12), P12008. –P12008. doi:10.1088/1748-0221/11/12/p12008

Azmoun, B., Caccavano, A., Rumore, M., Sinsheimer, J., Smirnov, N., Stoll, S., et al. (2010). A measurement of the scintillation light yield in ${\rm CF}_{4}$ using a photosensitive GEM detector. *IEEE Trans. Nucl. Sci.* 57, 2376–2381. doi:10.1109/tns.2010.2052632

Bai, C., Wang, L., Wan, H., Li, L., Liu, L., and Pan, J. (2018). Effects of CF_4 content on particle densities and reaction pathways in atmospheric-pressure Ar/CF_4 pulsed dielectric barrier discharge plasma. *J. Phys. D Appl. Phys.* 51, 255201. doi:10.1088/1361-6463/aac3e7

Baracchini, E., Benussi, L., Bianco, S., Capoccia, C., Caponero, M., Cavoto, G., et al. (2020). Stability and detection performance of a GEM-based Optical Readout TPC with He/CF4 gas mixtures. *J. Instrum.* 15 (10), P10001. doi:10.1088/1748-0221/15/10/p10001

Battat, J. B. R., Deaconu, C., Druitt, G., Eggleston, R., Fisher, P., Giampa, P., et al. (2014). The Dark Matter Time Projection Chamber 4Shooter directional dark matter detector: calibration in a surface laboratory. *Nucl. Instrum. Methods Phys. Res. Sect. A Accel. Spectrom. Detect. Assoc. Equip.* 755, 6–19. doi:10.1016/j.nima.2014.04.010

Berger, M. J., Hubbell, J. H., Seltzer, S. M., Chang, J., Coursey, J. S., Sukumar, R., et al. (2010). *XCOM: photon cross section database*. Gaithersburg, MD: National Institute of Standards and Technology. version 1.5, [Online] Available at: http://physics.nist.gov/xcom April 17, 2023).

Bi, Z.-H., Dai, Z. L., Xu, X., Li, Z. C., and Wang, Y. N. (2009). Numerical results for the Ar and CF_4 mixture gas in a dual frequency capacitively coupled plasma using a hybrid model. *Phys. Plasmas* 16, 043510. doi:10.1063/1.3125303

Boutillon, M. (1998). Volume recombination parameter in ionization chambers. *Phys. Med. Biol.* 43 (8), 2061–2072. doi:10.1088/0031-9155/43/8/005

Brunbauer, F. M., Galgóczi, G., Gonzalez Diaz, D., Oliveri, E., Resnati, F., Ropelewski, L., et al. (2018). Live event reconstruction in an optically read out GEM-based TPC. *Nucl. Instrum. Methods Phys. Res. Sect. A Accel. Spectrom. Detect. Assoc. Equip.* 886, 24–29. doi:10.1016/j.nima.2017.12.077

Buzulutskov, A., Shemyakina, E., Bondar, A., Dolgov, A., Frolov, E., Nosov, V., et al. (2018). Revealing neutral bremsstrahlung in two-phase argon electroluminescence. *Astropart. Phys.* 103, 29–40. doi:10.1016/j.astropartphys.2018.06.005

Christophorou, L. G., and Olthoff, J. K. (2004). *Fundamental electron interactions with plasma processing gases*. New York, NY: Kluwer Academic/Plenum Publishers.

Christophorou, L. G., Olthoff, J. K., and Rao, M. V. V. S. (1996). Electron interactions with CF4. *J. Phys. Chem. Reference Data* 25 (5), 1341–1388. doi:10.1063/1.555986

COMSOL (2023). *COMSOL Multiphysics®*. Stockholm, Sweden: COMSOL AB. www.comsol.com.

Connor, T. R., and Biondi, M. (1965). Dissociative recombination in neon: spectral line-shape studies. *Phys. Rev.* 140, A778–A791. doi:10.1103/physrev.140.a778

Fraga, F. A. F., Margato, L., Fetal, S., Fraga, M., Ferreira Marques, R., Policarpo, A., et al. (2002). CCD readout of GEM-based neutron detectors. *Nucl. Instrum. Methods Phys. Res. Sect. A Accel. Spectrom. Detect. Assoc. Equip.* 478, 357–361. doi:10.1016/s0168-9002(01)01829-0

Fraga, M. M. F. R., Fraga, F. A. F., Fetal, S. T. G., Margato, L. M. S., Marques, R. F., and Policarpo, A. J. P. L. (2003). The GEM scintillation in He–CF4, Ar–CF4, Ar–TEA and Xe–TEA mixtures. *Nucl. Instrum. Methods Phys. Res. Sect. A Accel. Spectrom. Detect. Assoc. Equip.* 504 (1–3), 88–92. doi:10.1016/s0168-9002(03)00758-7

Fraga, M. M. R., Bueno, C. C., Gonçalves, J. A. C., Fraga, F. A. F., Ferreira Marques, R., and Policarpo, A. J. P. L. (2001). Pressure dependence of secondary NIR scintillation in Ar and Ar/CF/sub 4/. *IEEE Trans. Nucl. Sci.* 48 (3 I), 330–335. doi:10.1109/23.940075

Frommhold, L., and Biondi, M. A. (1969). Interferometric study of dissociative recombination radiation in neon and argon afterglows. *Phys. Rev.* 185, 244–252. doi:10.1103/physrev.185.244

González-Díaz, D. (2016). *A survey on GEM-based readouts and gas mixtures for optical TPCs*. Vienna. Conference https://indico.cern.ch/event/391665/contributions/1827205/.

González-Díaz, D., Monrabal, F., and Murphy, S. (2018). Gaseous and dual-phase time projection chambers for imaging rare processes. *Nucl. Instrum. Methods Phys. Res. Sect. A Accel. Spectrom. Detect. Assoc. Equip.* 878, 200–255. doi:10.1016/j.nima.2017.09.024

Gutsev, G. L., and Adamowicz, L. (1995). The structure of the CF−4 anion and the electron affinity of the CF4 molecule{\mathrm{CF}}_{4}^- anion and the electron affinity of the CF_4 molecule. *J. Chem. Phys.* 102, 9309–9314. doi:10.1063/1.468797

Harshbarger, W. R., Robin, M. B., and Lassettre, E. N. (1972). The electron impact spectra of the fluoromethanes. *J. Electron Spectrosc. Relat. Phenom.* 1 (4), 319–332. doi:10.1016/0368-2048(72)80035-5

Henriques, C. A. O., Amedo, P., Teixeira, J., González-Díaz, D., Azevedo, C., Para, A., et al. (2022). Neutral Bremsstrahlung emission in xenon unveiled. *Phys. Rev. X* 12 (2), 021005. doi:10.1103/physrevx.12.021005

Jaffé, G. (1913). Zur theorie der Ionisation in kolonnen. *Ann. Phys.* 347, 303–344. doi:10.1002/andp.19133471205

Kumar, S. V. K., Rahman, M., and Roy, S. (2008). Anion formation by electron impact from CF_4. *Int. J. Mass Spectrom.* 277, 57–61. doi:10.1016/j.ijms.2008.05.014

Lambert, I. R., Mason, S. M., Tuckett, R. P., and Hopkirk, A. (1988). Decay pathways of excited electronic states of Group IV tetrafluoro and tetrachloro molecular ions studied with synchrotron radiation. *J. Chem. Phys.* 89 (5), 2683–2690. doi:10.1063/1.455019

Lee, L. C., Wang, X., and Suto, M. (1986). Fluorescence from extreme ultraviolet photoexcitation of CF4. *J. Chem. Phys.* 85 (11), 6294–6300. doi:10.1063/1.451459

Lehaut, G., Salvador, S., Fontbonne, J. M., Lecolley, F. R., Perronnel, J., and Vandamme, C. (2015). Scintillation properties of N2 and CF4 and performances of a scintillating ionization chamber. *Nucl. Instrum. Methods Phys. Res. Sect. A Accel. Spectrom. Detect. Assoc. Equip.* 797, 57–63. doi:10.1016/j.nima.2015.05.050

Liu, J., Ouyang, X., Chen, L., Zhang, X., Liu, J., Zhang, Z., et al. (2012). Primary scintillation characteristics of Ar+CF4 gas mixtures excited by proton and alpha particles. *Nucl. Instrum. Methods Phys. Res. Sect. A Accel. Spectrom. Detect. Assoc. Equip.* 694, 157–161. doi:10.1016/j.nima.2012.08.018

Manly, S., Kordosky, M., and On behalf of the DUNE Collaboration (2021). Deep underground neutrino experiment (DUNE) near detector conceptual design report. *Instruments* 5 (4), 31. doi:10.3390/instruments5040031

Margato, L. M. S., Morozov, A., Pereira, L., Fraga, M. M. F. R., and Fraga, F. A. F. (2012). Effect of the gas contamination on CF4 primary and secondary scintillation. *Nucl. Instrum. Methods Phys. Res. Sect. A Accel. Spectrom. Detect. Assoc. Equip.* 695, 425–428. doi:10.1016/j.nima.2011.10.033

Maslaáni, A., and Sember, V. (2014). Emission spectroscopy of OH radical in water-argon arc plasma jet. *J. Spectrosc.* 952138. doi:10.1155/2014/952138

Menzel, H.-G. (2014). ICRU (report 90), key data for ionizing-radiation dosimetry: measurement standards and applications, Volume 14, 1.

Morozov, A., Fraga, M., Pereira, L., Margato, L., Fetal, S., Guerard, B., et al. (2010). Photon yield for ultraviolet and visible emission from CF4 excited with alpha particles. *Nucl. Instrum. Methods Phys. Res. Sect. B Beam Interact. Mater. Atoms* 268 (9), 1456–1459. doi:10.1016/j.nimb.2010.01.012

Morozov, A., Fraga, M., Pereira, L., Margato, L., Fetal, S., Guerard, B., et al. (2011). Effect of the electric field on the primary scintillation from CF_4. *Nucl. Instrum. Methods Phys. Res. Sect. A Accel. Spectrom. Detect. Assoc. Equip.* 628 (1), 360–363. doi:10.1016/j.nima.2010.07.001

Morozov, A., Margato, L. M. S., Fraga, M. M. F. R., Pereira, L., and Fraga, F. A. F. (2012). Secondary scintillation in CF4: emission spectra and photon yields for MSGC and GEM. *J. Instrum.* 7 (2), P02008. doi:10.1088/1748-0221/7/02/p02008

Müller, U., Bubel, Th., and Schulz, G. (1993). Electron impact dissociation of H_3O: emission cross sections for OH*, OH**,H* and {\mathrm{H}}_{2}{+\ast }O. *Z Phys D - Atoms, Mol. Clust.* 25, 167–174. doi:10.1007/bf01450171

Nygren, D. (2023). *The Time Projection Chamber - a new 4π detector for charged particles*. PEP-144-1974.

Onsager, L. (1938). Initial recombination of ions. *Phys. Rev.* 54, 554–557. doi:10.1103/physrev.54.554

Palestini, S., and McDonald, K. T. (2023). Space charge in ionization detectors. http://kirkmcd.princeton.edu/examples/spacecharge.pdf.

Pansky, A., Breskin, A., Buzulutskov, A., Chechik, R., Elkind, V., and Va'vra, J. (1995). The scintillation of CF4 and its relevance to detection science. *Nucl. Instrum. Methods Phys. Res. Sect. A Accel. Spectrom. Detect. Assoc. Equip.* 354 (2–3), 262–269. doi:10.1016/0168-9002(94)01064-1

Pomorski, M., Pfützner, M., Dominik, W., Grzywacz, R., Stolz, A., Baumann, T., et al. (2014). Proton spectroscopy of Ni 48, Fe 46, and Cr 44. *Phys. Rev. C* 90, 014311–014312. doi:10.1103/physrevc.90.014311

Reader, J., Corliss, C. H., Wiese, W. L., and Martin, G. A. (1980). *Natl. Stand. Ref. Data Ser. Natl. Bur. Stand. (U.S.)* 68.

Reinking, G. F., Christophorou, L. G., and Hunter, S. R. (1986). Studies of total ionization in gases/mixtures of interest to pulsed power applications. *J. Appl. Phys.* 60 (2), 499–508. doi:10.1063/1.337792

Robert, E., Khacef, A., Cachoncinlle, C., and Pouvesle, J. M. (1995). Time-resolved spectroscopy of high pressure rare gases excited by an energetic flash X-ray source. *Opt. Commun.* 117, 179–188. doi:10.1016/0030-4018(94)00664-g

Saá-Hernández, A., González-Díaz, D., Martín-Albo, J., Tuzi, M., Amedo, P., Benítez, C., et al. (2023). *On the determination of the interaction time of GeV-neutrinos in large argon-gas TPCs, on preparation for submission to JHEP*.

Santorelli, R., Garcia, E. S., Abia, P. G., González-Díaz, D., Manzano, R. L., Morales, J. J. M., et al. (2021). Spectroscopic analysis of the gaseous argon scintillation with a wavelength sensitive particle detector. *Eur. Phys. J. C* 81, 622. doi:10.1140/epjc/s10052-021-09375-3

Santos, M. A. G., Kaja, M., Cortez, A., Veenhof, R., Neves, P., Santos, F., et al. (2018). Experimental ion mobility measurements for the LCTPC collaboration—Ar-CF_4 mixtures. *J. Instrum.* 13, P04012. doi:10.1088/1748-0221/13/04/p04012

Smirnov, I. B. (2005). Modeling of ionization produced by fast charged particles in gases. *Nucl. Instrum. Methods Phys. Res. Sect. A Accel. Spectrom. Detect. Assoc. Equip.* 554 (1–3), 474–493. doi:10.1016/j.nima.2005.08.064

Strickler, T. D., and Arakawa, E. T. (1964). Optical emission from argon excited by alpha particles: quenching studies. *J. Chem. Phys.* 41 (6), 1783–1789. doi:10.1063/1.1726158

Suto, M., Washida, N., Akimoto, H., and Nakamura, M. (1983). Emission spectra of CF 3 radicals. III. Spectra and quenching of CF 3 emission bands produced in the VUV photolyses of CF 3 Cl and CF 3 Br. *J. Chem. Phys.* 78 (3), 1019–1024. doi:10.1063/1.444901

Takahashi, M., Kabuki, S., Hattori, K., Higashi, N., Iwaki, S., Kubo, H., et al. (2011). Development of an Electron-Tracking Compton Camera using CF4 gas at high pressure for improved detection efficiency. *Nucl. Instrum. Methods Phys. Res. Sect. A Accel. Spectrom. Detect. Assoc. Equip.* 628 (1), 150–153. doi:10.1016/j.nima.2010.06.305

Takahashi, T., Himi, S., Suzuki, M., Ruan(Gen, J., and Kubota, S. (1983). Emission spectra from Ar-Xe, Ar-Kr, Ar-N_2, Ar-CH_4, Ar-CO_2 and Xe-N_2 gas scintillation proportional counters. *Nucl. Instrum. Methods Phys. Res.* 205, 591–596. doi:10.1016/0167-5087(83)90028-5

Toneli, D. A., Pessoa, R. S., Roberto, M., and Gudmundsson, J. T. (2019). A global model study of low pressure high density CF_4 discharge. *Plasma Sources Sci. Technol.* 28, 025007. doi:10.1088/1361-6595/aaf412

Velazco, J. E., Kolts, J. H., and Setser, D. W. (1978). Rate constants and quenching mechanisms for the metastable states of argon, krypton, and xenon. *J. Chem. Phys.* 69 (10), 4357–4373. doi:10.1063/1.436447

Walter, B., Riefler, W., and Roland, L. (2008). *Particle detection with drift chambers*. Heidelberg: Springer Berlin.

Washida, N., Suto, M., Nagase, S., Nagashima, U., and Morokuma, K. (1983). Emission spectra of CF3 radicals. IV. Excitation spectra, quantum yields, and potential energy surfaces of the CF3 fluorescences. *J. Chem. Phys.* 78 (3), 1025–1032. doi:10.1063/1.444902

Wieser, J., Ulrich, A., Fedenev, A., and Salvermoser, M. (2000). Novel pathways to the assignment of the third rare gas excimer continua. *Opt. Commun.* 173, 233–245. doi:10.1016/s0030-4018(99)00610-0

Winters, H. F., and Inokuti, M. (1982). Total dissociation cross section of CF4 and other fluoroalkanes for electron impact. *Phys. Rev. A* 25, 1420–1430. doi:10.1103/physreva.25.1420

Zhang, W., Cooper, G., Ibuki, T., and Brion, C. E. (1989). Excitation and ionization of freon molecules. I. Absolute oscillator strengths for the photoabsorption (12–740 eV) and the ionic photofragmentation (15–80 ev) of CF4. *Chem. Phys.* 137 (1–3), 391–405. doi:10.1016/0301-0104(89)87122-8

Ziegler, J. F., Ziegler, M. D., and Biersack, J. P. (2010). SRIM - the stopping and range of ions in matter. *Nucl. Instrum. Methods Phys. Res. Sect. B Beam Interact. Mater. Atoms* 268 (11–12), 1818–1823. doi:10.1016/j.nimb.2010.02.091

Zimmerman, W. R. (2023). Direct observation of the second 2+ state in 12C. PhD Thesis. https://opencommons.uconn.edu/dissertations/230/.